Earth and Planetary Science Letters 475 (2017) 169–180

Contents lists available at ScienceDirect

Earth and Planetary Science Letters

www.elsevier.com/locate/epsl

Sr and O isotopes in western Aleutian seafloor lavas: Implications for the source of fluids and trace element character of arc volcanic rocks

Gene M. Yogodzinski [a,*], Peter B. Kelemen [b], Kaj Hoernle [c], Shaun T. Brown [a,d], Ilya Bindeman [e], Jeffrey D. Vervoort [f], Kenneth W.W. Sims [g], Maxim Portnyagin [c,h], Reinhard Werner [c]

[a] School of Earth, Ocean, and Environment, University of South Carolina, 701 Sumter St., EWSC617, Columbia, SC 29208, USA
[b] Lamont-Doherty Earth Observatory, Columbia University, 61 Route 9W, Palisades, NY 10964, USA
[c] GEOMAR – Helmholtz Centre for Ocean Research, Kiel Wischhofstrasse 1-3, D-24148 Kiel, Germany
[d] Energy Geosciences Division, E.O. Lawrence Berkeley National Laboratory, 1 Cyclotron Rd MS 70A-4418, Berkeley, CA 94720, USA
[e] Department of Geological Sciences, University of Oregon, 1275 East 13th Avenue, Eugene, OR, 97403-1272, USA
[f] School of Earth & Environmental Sciences, Washington State University, P.O. Box 642812, Pullman, WA 99164-6376, USA
[g] Department of Geology & Geophysics, University of Wyoming, 1000 East University Avenue, Laramie, WY 82071-2000, USA
[h] V.I. Vernadsky Institute of Geochemistry and Analytical Chemistry, Kosigin st. 19, 119991 Moscow, Russia

ARTICLE INFO

Article history:
Received 10 March 2017
Received in revised form 27 June 2017
Accepted 3 July 2017
Available online 31 July 2017
Editor: M. Bickle

Keywords:
subduction
petrology
geochemistry
trace elements
isotopes

ABSTRACT

High Mg# andesites and dacites (Mg# = molar Mg/Mg + Fe) from western Aleutian seafloor volcanoes carry high concentrations of Sr (>1000 ppm) that is unradiogenic ($^{87}Sr/^{86}Sr < 0.7029$) compared to lavas from emergent volcanoes throughout the arc (200–800 ppm Sr, $^{87}Sr/^{86}Sr > 0.7030$). Data patterns in plots of $^{87}Sr/^{86}Sr$ vs Y/Sr and Nd/Sr imply the existence of an eclogite-melt source component – formed by partial melting of MORB eclogite in the subducting Pacific Plate – which is most clearly expressed in the compositions of western Aleutian andesites and dacites (Nd/Sr and Y/Sr < 0.02) and which dominates the source budget for Sr in volcanic rocks throughout the arc. When viewed in combination with inversely correlated ε_{Nd} and $^{87}Sr/^{86}Sr$, these patterns rule out aqueous fluids as an important source of Sr because mixtures of fluids from altered oceanic crust with depleted mantle and sediment produce compositions with $^{87}Sr/^{86}Sr$ higher than in common Aleutian rocks. The unradiogenic nature of Sr in the western Aleutian andesite–dacite end-member may be understood if H_2O required to drive melting of the subducting oceanic crust is transported in fluids containing little Sr. Mass balance demonstrates that such fluids may be produced by dewatering of serpentinite in the mantle section of the subducting plate. If the eclogite-melt source component is present throughout the Aleutian arc, melting of the subducting plate must extend into minimally altered parts of the sheeted dike section or upper gabbros, at depths >2 km below the paleo-seafloor. Oxygen isotopes in western Aleutian seafloor lavas, which fall within a narrow range of MORB-like values ($\delta^{18}O = 5.1–5.7$), are also consistent with this model. These results indicate that the subducting Pacific lithosphere beneath the Aleutian arc is significantly hotter than indicated my most thermal models.

1. Introduction

The source of island-arc magmas is widely viewed as a mixture of upper mantle and recycled components derived from seawater, subducted basalt and marine sediment. The element Sr provides unique constraints on subduction magma source models, because it is a fluid-mobile element that is both abundant and relatively unradiogenic in arc rocks. This is particularly clear in the Aleutians, where basalts commonly have 400–500 ppm Sr and Sr/Nd of 30–50, indicating 3-times higher Sr/Nd than similarly evolved MORB (~5–10% MgO), which typically have 85–150 ppm Sr and Sr/Nd = 5–20. Despite these strong enrichments, Aleutian basalts have $^{87}Sr/^{86}Sr$ that is offset from MORB only slightly (median Aleutian $^{87}Sr/^{86}Sr$ ~0.7032 versus ~0.7028 in global MORB). Hawkesworth et al. (1993) and others have noted that arc vol-

* Corresponding author.
E-mail addresses: gyogodzin@geol.sc.edu (G.M. Yogodzinski), peterk@ldeo.columbia.edu (P.B. Kelemen), khoernle@geomar.de (K. Hoernle), stbrown@lbl.gov (S.T. Brown), bindeman@uoregon.edu (I. Bindeman), vervoort@wsu.edu (J.D. Vervoort), ksims7@uwyo.edu (K.W.W. Sims), mportnyagin@geomar.de (M. Portnyagin), rwerner@geomar.de (R. Werner).

http://dx.doi.org/10.1016/j.epsl.2017.07.007
0012-821X/

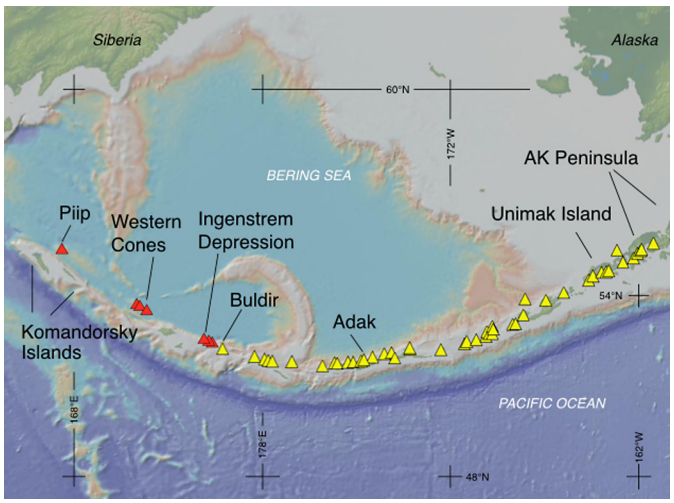

Fig. 1. Map of north Pacific and Bering, showing Aleutian locations mentioned in the text. Yellow triangles mark the locations of emergent volcanoes on Aleutian islands. Red triangles indicate the locations of western Aleutian seafloor volcanoes (see also Yogodzinski et al., 2015 for more detailed maps of western Aleutian seafloor volcanic structures). (For interpretation of the references to color in this figure legend, the reader is referred to the web version of this article.)

canic rocks globally with high Sr abundances commonly carry relatively unradiogenic $^{87}Sr/^{86}Sr$. These patterns imply that there is an abundant source of unradiogenic Sr in arc rocks, which is not present in MORB. This source is generally inferred to be from a subducted/recycled source (e.g., Hawkesworth et al., 1979; Kay, 1980). This presents a puzzle because abundant sources of subducted Sr lie predominantly in sediment (GLOSS $^{87}Sr/^{86}Sr$ = 0.712 to 0.717) and altered oceanic crust (AOC $^{87}Sr/^{86}Sr \sim 0.705$, Staudigel, 2003 and references therein), both of which are more radiogenic than average island arc basalt ($^{87}Sr/^{86}Sr \sim 0.7034$, Hawkesworth et al., 1991).

In this paper, we explore the implications of seafloor lavas from the western Aleutian arc with respect to the source of Sr and geochemically related trace elements. We focus on high-Sr (adakitic) andesites and dacites from the western Aleutians, because formation of these rocks involves small degrees of fluid-saturated melting of MORB eclogite, which creates a Sr-rich, geochemical component that is present in volcanic rocks throughout the Aleutian arc (Yogodzinski et al., 2015 and references therein). New Sr and oxygen isotope data presented in this paper are consistent with previous findings which indicate that the eclogite melt source component is a major carrier of incompatible trace elements present in Aleutian volcanic rocks (e.g., Kelemen et al., 2003b; Yogodzinski and Kelemen, 1998). Results presented here also indicate that H_2O-bearing fluids required to drive melting of the subducting oceanic crust are likely to have carried little Sr and may have been produced by dehydration of serpentinite in the mantle section of the subducting lithosphere.

2. Samples, data, and background

The western Aleutian seafloor lavas were collected by dredging from the Ingenstrem Depression and Western Cones areas (Fig. 1) with the U.S. *R/V Thompson* during Western Aleutian Volcano Expedition in 2005 (The WAVE), and with the German *R/V Sonne*, during KALMAR and BERING cruises in 2009 and 2016 (SO201-1b, SO249-1). Here, we refer to the Ingenstrem and Western Cones samples collectively as the *western Aleutian seafloor lavas*. In this paper we present new, whole-rock Sr isotope ratio measurements on 54 samples as well as 32 oxygen and 10 hydrogen isotope measurements on mineral separates from 12 rocks.

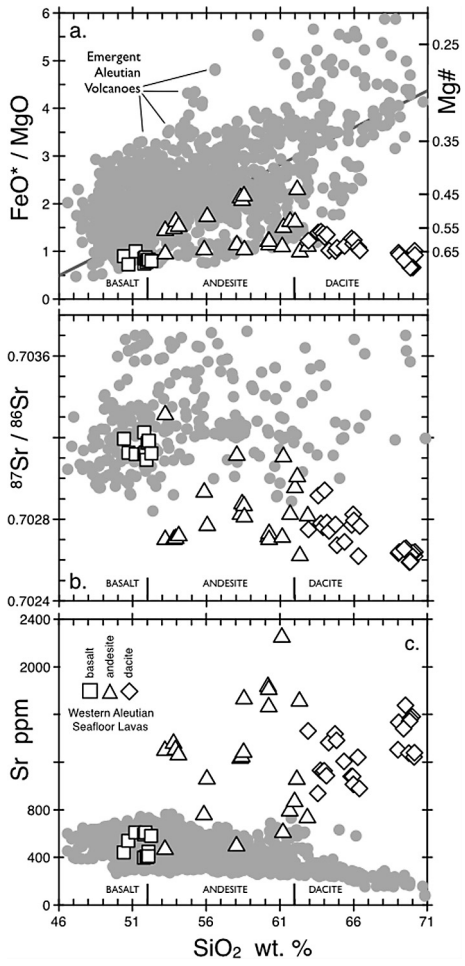

Fig. 2. Aleutian whole-rock compositions. Large, open symbols are western Aleutian seafloor lavas from Yogodzinski et al. (2015). Gray symbols are published data for samples from emergent Aleutian volcanoes collected at locations from the western tip of the Alaska Peninsula to Buldir Island (Fig. 1). These data are from the compilation of Kelemen et al. (2003b) updated to include more recently published data. (a) FeO^*/MgO versus SiO_2 with right vertical axis showing Mg# calculated on a molar basis and total iron as Fe^{2+}. The black diagonal line across the plot is the calc-alkaline (CA) – tholeiitic (TH) discriminant line of Miyashiro (1974). (b) $^{87}Sr/^{86}Sr$ and (c) Sr abundance. Strontium isotope data are from Table 1. Complete major element and trace element data (except for SO249 samples) are available in Yogodzinski et al. (2015).

Western Aleutian lavas define a highly calc-alkaline igneous series from 50 to 70% SiO_2 in which most rocks have Mg# >0.60 (Fig. 2a). If such a series was created by fractional crystallization, hydrous and likely oxidizing conditions during basalt formation and evolution would be required (e.g., Sisson and Grove, 1993). In fact, petrographic observations indicate that pre-eruptive H_2O contents were high (Yogodzinski et al., 2015). However, because isotopic compositions change systematically toward more depleted compositions with increasing SiO_2 the western Aleutian series cannot be interpreted as primarily the product of fractional crystallization. The series has instead, been interpreted as the product of the interaction between hydrous and silicic partial melts of subducting MORB eclogite with hotter peridotite and basalt in the overlying mantle wedge (Yogodzinski et al., 2015 and references therein). A brief review of key aspects of this and alternative interpretations is provided here.

The key rocks in the western Aleutian series are the high-silica dacites (rhyodacites) which have ~69% SiO_2, ~2% MgO, Mg# >0.65 and highly fractionated trace element patterns with Sr > 1000 ppm and low abundance of heavy REEs (rare earth elements) requiring a role for residual garnet. These characteristics

are nothing like what we find in rhyolites of the Izu–Bonin arc, or in Icelandic rhyolites or other forms of high-silica ocean-ridge volcanism, which may form either by extensive fractional crystallization or by partial melting of mafic crust (e.g., Lacasse et al., 2007; Tamura et al., 2009; Wanless et al., 2010).

Melting at the base of a mafic crust is a viable model for creating high-silica magmas in some arcs, but this model fails in the western Aleutians because the volcanoes that produce the rhyodacites are constructed on oceanic crust of the Bering Sea, which is unlikely to be more than 10 km thick. This is important because residual garnet is required in the interpretation of the trace element data, but the physical conditions that stabilize garnet during melting reactions will not be realized at such shallow depths (see Yogodzinski et al., 2015 for citations and additional discussion). The need for residual garnet derives from strong fractionation of the middle/heavy parts of the REE pattern, resulting in high Gd/Yb (Fig. 8b in Yogodzinski et al., 2015). The distinctive shape of the REE patterns in the rhyodacites likely reflects the LREE-depleted pattern in the source rock (MORB), which has been rotated clockwise from the effects of residual garnet. This results in low abundances of heavy REEs, enrichment in the light REEs, and a flattening at both ends to create a sigmoidal shape in the REE pattern, as described by O'Neill (2016) but without a role for residual amphibole.

More broadly, the western Aleutians is an unlikely place to produce high-silica rocks by melting of the arc crust, because low magmatic output of the subduction zone fails to provide a viable source of heat to drive melting, as seen in other parts of the Alaska–Aleutian system (e.g., Hildreth and Fierstein, 2000). In contrast, an interpretation that involves melting of the subducting plate is clearly linked to a tectonic setting of oblique convergence in the western Aleutians which produces a relatively hot subducting plate (Yogodzinski et al., 1995, 1994) as well as a cool and perhaps stagnant mantle wedge compared to the central and eastern Aleutians, where advection of hot peridotite into the wedge corner is driven by higher subduction rates (Kelemen et al., 2003b; Yogodzinski et al., 2015). Thus, the combined geologic setting and geochemical data favor models that involve melting of MORB eclogite of the subducting plate and appear to leave no viable alternatives (Yogodzinski et al., 2015 and references therein).

3. Analytical methods

Strontium isotope ratios reported here were determined in laboratories at Washington State University, the Woods Hole Oceanographic Institution, and the University of South Carolina. All results are corrected to an $^{87}Sr/^{86}Sr$ value of 0.710240 for the NBS987 Sr isotope standard. Analytical procedures used in these laboratories and external precision based on repeat analyses of standards are summarized below. References to publications containing additional analytical information are also provided.

At South Carolina, rock powders used for Sr isotope analyses were leached with 6 M HCl in Teflon capsules at ~120 °C for one hour. The leached samples were digested in 4 mL of an HF:HNO_3 mixture (3:1). The samples were dried and re-dissolved in ~5 ml of 6 M HCl and then heated at ~95 °C to incipient dryness to remove precipitates. Samples were then dissolved in 2.5 N HCl and centrifuged for 10 min at 40,000 rpm. The centrifuged samples were loaded onto a ~5 mL bed of cation-exchange resin (200–400 μm Eichrom 50W-X8) in Teflon columns. The Sr fraction was separated from the rock matrix by elution in 2.5 N HCl. Strontium fractions were dried, dissolved in 0.001 N HNO_3 and loaded on an Eichrom SR-B50-S resin in Teflon micro-columns. The samples were rinsed with 3.5 N HNO_3 and separated from the resin with 0.001 N HNO_3. Isotope ratios were measured on the Thermo Fisher Neptune in the Center for Elemental Mass Spectrometry. Results were normalized to $^{86}Sr/^{88}Sr = 0.1194$.

At Washington State, samples were prepared from aliquots of whole-rock powders and were dissolved at high pressure in steel-jacketed Teflon bombs in a 10:1 mixture of concentrated Hf and HNO_3 at 150 °C for 5–7 days. Samples were initially separated on cation exchange columns using AG 50W-X8 resin (200–400 mesh) and were purified using micro-columns (0.18 ml rein volume) with Sr-spec resin and HNO_3. Analyses were made using a Thermo-Finnigan Neptune multicollector (MC)-ICP-MS system. Results were corrected for mass fractionation using $^{86}Sr/^{88}Sr = 0.1194$ and normalized to NBS-987. Uncertainties listed in Table 1 reflect in-run error only, presented as two standard errors.

At WHOI, Sr isotope samples were prepared according to the details outlined in the supplemental information of Sims et al. (2013). Rock powders were leached for ~1 h in hot 6.2 M HCl, and then rinsed repeatedly with 18 MΩ H_2O. Leached powders were dissolved in a concentrated HF:$HClO_4$ mixture, followed by conversion of fluorides to chlorides by drying down three times with 6.2 N HCl. Strontium separation was done by conventional ion-exchange chromatography using DOWEX 50 cation-exchange resin. The total procedural blank for Sr was <400 pg. All Sr isotopes were measured at WHOI by MC-ICPMS using the ThermoFinnigan NEPTUNE. Strontium isotopic ratios were normalized for instrumental mass fractionation relative to $^{86}Sr/^{88}Sr = 0.1194$ also using an exponential law. For Sr isotopic measurements, the internal precision was 5–10 ppm (2σ). The external precision, after adjusting to 0.710240 for the NBS987 Sr standard was <30 ppm (2σ) for Sr.

Oxygen isotope analyses were performed by laser fluoridation using a 35 W New Wave laser on one or two mineral grains (1.2–1.5 mg) using purified BrF_5 as a reactant. Generated gases were passed through a series of cryogenic traps cooled by liquid nitrogen, and a hot Hg diffusion pump to strip away excess F_2 gas resulting from disproportionation of the reagent upon lasing. Oxygen (O_2) was converted to CO_2 using a small Pt–C converter and yields of generated gas were measured. Analyses were run on a MAT253 gas source mass spectrometer connected to the laser fluorination-vacuum line. The San Carlos olivine ($\delta^{18}O = 5.25‰$) and Gore Mountain garnet ($\delta^{18}O = 5.75‰$) standards were run to calibrate day-to-day variation and to normalize the data to the SMOW scale with an offset 0.0‰. The uncertainty in the $\delta^{18}O$ measurement is 0.10‰ based on repeat analyses of standards run with unknowns. For hydrogen isotopes of amphibole separates, we used a glassy carbon TC/EA continuous flow system at 1450 °C integrated by helium flow to the MAT253 mass spectrometer. Analytical standards (USGS57, USGS58, NBS30) were run concurrently with the unknowns. Values for δD are calibrated relative to SMOW using the USGS57 and USGS58 mica standards. Uncertainties on the standards were ±1.5‰ δD and 0.11 wt% H_2O. Additional details about the method may be found in Bindeman et al. (2012).

4. Results

Strontium isotope compositions of western Aleutian seafloor lavas (Table 1) change systematically with SiO_2. Basalts have $^{87}Sr/^{86}Sr \sim 0.70315$, which is a typical for basalts throughout the arc. At higher silica the trend is toward less radiogenic Sr. Dacites with SiO_2 >67% are the least radiogenic with $^{87}Sr/^{86}Sr$ from 0.70259 to 0.70263 (Fig. 2b). These are among the lowest Sr isotope ratios observed in arc magmas, and they are coupled with the some of the highest Nd and lowest Pb isotope ratios in arc lavas worldwide (Kelemen et al., 2003a; Yogodzinski et al., 2015). Most western Aleutian seafloor lavas have high Sr (>800 ppm) at intermediate and high-silica contents (Fig. 2c) and show progressively lower $^{87}Sr/^{86}Sr$ with increasing

Table 1
Whole-rock Sr isotope results.

Field ID	IGSN	SiO_2 (wt.%)	Sr (ppm)	Laboratory[a]	$^{87}Sr/^{86}Sr$[b]	2σ[c,d]	Field ID	IGSN	SiO_2	Sr (ppm)	Laboratory[a]	$^{87}Sr/^{86}Sr$[b]	2σ[c,d]
SO201-1b-09-001		53.2	1306	SCAR	0.702705	±6	SO201-1b-10-011		62.0	879	SCAR	0.702960	±6
SO201-1b-09-002		52.7	1377	SCAR	0.702702	±6	SO201-1b-09-011		62.2	1063	SCAR	0.703013	±8
SO201-1b-09-005		53.8	1367	SCAR	0.702705	±8	SO201-1b-20-005		62.3	1721	SCAR	0.702627	±6
SO201-1b-09-007		56.0	1067	SCAR	0.702774	±8	TN182_01_004	GMY00002L	62.8	743	WSU	0.702821	±12
SO201-1b-09-008		58.6	1740	SCAR	0.702816	±6	SO201-1b-09-014		62.9	1462	SCAR	0.702750	±6
SO201-1b-09-010		61.2	618	SCAR	0.703111	±8	TN182_03_004	GMY00002U	63.6	937	WHOI	0.702916	
SO201-1b-10-003		53.9	1315	SCAR	0.702712	±8	TN182_03_005	GMY00002V	63.7	1130	WHOI	0.702780	
SO201-1b-10-005		54.1	1269	SCAR	0.702724	±6	TN182_03_008	GMY00002Y	63.9	1117	WSU	0.702761	±10
SO201-1b-10-010		61.7	800	SCAR	0.702830	±8	TN182_03_002	GMY00002S	64.0	1162	WSU	0.702942	±10
SO201-1b-14-006		52.3	582	SCAR	0.703122	±6	TN182_03_009	GMY00002Z	64.2	1085	WSU	0.702783	±16
SO201-1b-14-007		50.7	539	SCAR	0.703126	±6	TN182_07_009	GMY00003H	64.3	1365	WHOI	0.702743	
SO201-1b-14-008		51.2	610	SCAR	0.703118	±4	TN182_07_004	GMY00003C	64.7	1436	WHOI	0.702774	
SO201-1b-15-001		51.8	593	SCAR	0.703120	±6	TN182_07_005	GMY00003D	64.9	1384	WSU	0.702672	±10
SO201-1b-16-007		51.9	610	SCAR	0.703127	±6	TN182_04_004	GMY000034	65.3	1207	SCAR	0.702689	±6
TN182_05_001	GMY000035	55.8	767	WHOI	0.702937		TN182_01_006	GMY00002N	65.8	1081	WSU	0.702772	±14
TN182_07_002	GMY00003A	52.0	405	WHOI	0.703173		TN182_01_001	GMY00002I	65.9	1081	WHOI	0.702824	
TN182_08_003	GMY00003M	51.8	398	WHOI	0.703225		TN182_01_003	GMY00002K	66.0	1014	WSU	0.702795	±12
TN182_08_013	GMY00003W	51.9	408	WSU	0.703091	±16	TN182_04_003	GMY000033	66.3	1241	WSU	0.702620	±10
TN182_08_014	GMY00003X	52.1	448	WHOI	0.703182		TN182_01_007	GMY00002O	66.4	978	WSU	0.702767	±14
TN182_09_001	GMY000041	50.4	443	WHOI	0.703194		SO201-1b-36-007		69.0	1304	SCAR	0.702634	±6
TN182_10_001	GMY000047	58.5	1291	WHOI	0.702872		SO201-1b-34-002		69.0	1536	SCAR	0.702640	±5
TN182_10_002	GMY000048	58.4	1253	SCAR	0.702881	±6	SO201-1b-36-003		69.5	1677	SCAR	0.702657	±4
TN182_10_003	GMY000049	58.3	1240	WSU	0.702829	±10	SO201-1b-35-003		69.7	1277	SCAR	0.702589	±5
TN182_10_004	GMY00004A	60.2	2257	WSU	0.702717	±8	SO249-1-DR37-10	GMY0000S6	69.4	1482	SCAR	0.702654	±12
TN182_11_001	GMY00004C	60.2	1675	WHOI	0.702735		SO249-1-DR37-8	GMY0000SD	69.8	1544	SCAR	0.702592	±6
TN182_11_003	GMY00004E	60.2	1843	WHOI	0.702718		SO249-1-DR37-7	GMY0000SC	69.8	1565	SCAR	0.702595	±8
TN182_11_004	GMY00004F	58.0	506	WSU	0.703118	±11	SO249-1-DR37-6	GMY0000SB	69.8	1566	SCAR	0.702626	±12
TN182_11_005	GMY00004G	60.2	1819	WSU	0.702705	±10	SO249-DR37-01	GMY0000S5	70.0	1582	SCAR	0.702635	±12
TN182_13_001	GMY00004L	53.2	476	WHOI	0.703317		SO201-1b-35-004		70.1	1244	SCAR	0.702620	±4
TN182-08-006	GMY00003P	52.1	411	SCAR	0.703184	±5	SO201-1b-33-001		70.1	1280	SCAR	0.702640	±7

[a] WSU = Washington State University, WHOI = Woods Hole Oceanographic Institution, SCAR = University of South Carolina.
[b] $^{87}Sr/^{86}Sr$ is normalized to a reference value of 0.710240 for the NBS987 isotopes standard.
[c] Errors are within-run uncertainties calculated as two standard errors and expressed as variation in the last decimal place.
[d] Precision on $^{87}Sr^{86}Sr$ measurements at WHOI are ±10–20 ppm.

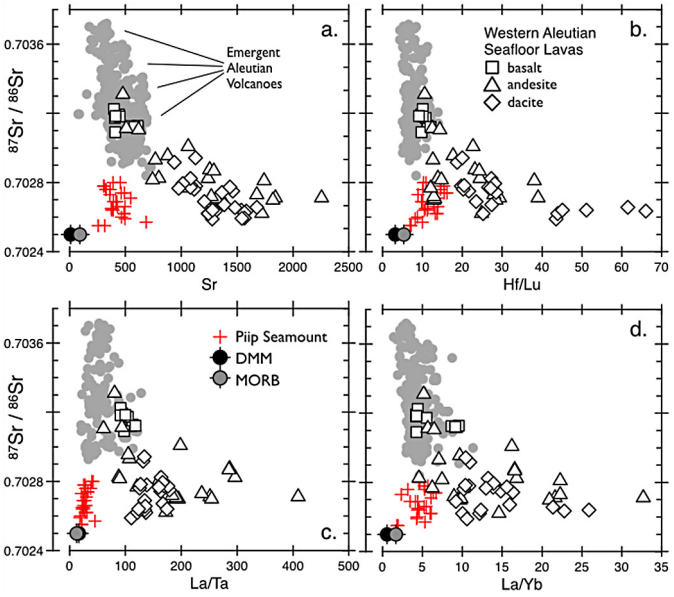

Fig. 3. Whole-rock $^{87}Sr/^{86}Sr$ in Aleutian volcanic rocks versus Sr (a), Hf/Lu (b), La/Ta (c) and La/Yb (d). In each panel, the trace element ratios on the horizontal axes places the eclogite-melt source component in the lower-right of the plots and depleted mantle and MORB in the lower-left. Sediment and seawater altered oceanic crust generally have $^{87}Sr/^{86}Sr > 0.7038$ and so are off-scale in the upper left. Data for Piip Seamount, located in the westernmost Aleutians (Fig. 1) are from Yogodzinski et al. (1994) and include pre-Piip (Komandor Series) samples. Other data sources are the same as in Fig. 3. MORB is the average of Juan de Fuca Ridge (northeast Pacific) data ($^{87}Sr/^{86}Sr = 0.7025$, La = 5.75 ppm, Yb = Y, Hf = 2.81, Lu = 0.519, Ta = 0.445, Sr = 134, Y = 34.3) from Gale et al. (2013). Average DMM trace elements are from Salters and Stracke (2003) with $^{87}Sr/^{86}Sr$ also reflecting Juan de Fuca MORB.

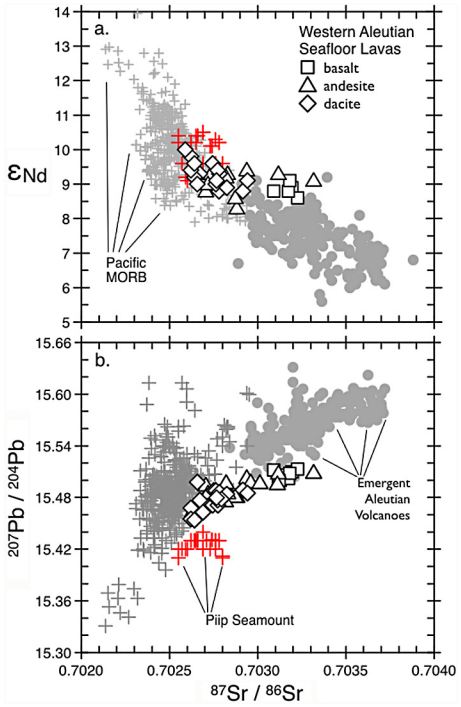

Fig. 4. Aleutian whole-rock isotopes compared with published Pacific MORB data. (a) ε_{Nd} versus $^{87}Sr/^{86}Sr$. (b) $^{207}Pb/^{204}Pb$ versus $^{87}Sr/^{86}Sr$. Data sources except Pacific MORB are the same as in Figs. 3–4. Pacific MORB data are from published sources.

SiO_2 (Fig. 2b). Like Sr, Pb and Nd isotope ratios also become more depleted with increasing SiO_2 from basalt to dacite (Yogodzinski et al., 2015). Strontium isotopes show an inverse correlation with Sr abundance, similar to the correlation between Sr isotopes and SiO_2 (Fig. 3a). Thus, low-Sr basalts have high Sr isotope ratios, while andesites and dacites with higher Sr concentrations have lower $^{87}Sr/^{86}Sr$ (Fig. 2). Other Aleutian lavas with similarly unradiogenic Sr are observed at Piip Volcano, which is a highly calc-alkaline center on the seafloor north of the Komandorsky Islands (Fig. 1). Samples from Piip include many high-Mg# andesites and dacites with low $^{87}Sr/^{86}Sr$ (<0.7028) but moderate Sr abundances (300–500 ppm) similar to basalts and andesites throughout the Aleutians (Fig. 3a).

In Nd–Sr isotope space, western Aleutian dacites with the least radiogenic Sr also have the most radiogenic Nd (ε_{Nd} up to +10.0). However, the dominant pattern for the western Aleutian samples is a flat trend, with ε_{Nd} falling mostly between +8.5 and +9.5 over a relatively wide range of Sr isotopes (Fig. 4a). This is particularly evident when the trend for the western seafloor lavas is compared to the whole Aleutian data field, which shows a strong inverse relationship for Nd and Sr isotopes (Fig. 4a). A similar pattern emerges for Pb isotopes, which are well correlated with $^{87}Sr/^{86}Sr$ but form a pattern that is slightly less steep than the main Aleutian array (Fig. 4b).

Oxygen isotopes were measured on mineral separates (primarily olivine and amphibole) from 12 western Aleutian rocks (Table 2). Amphibole analyses were adjusted downward by 0.4‰ to create olivine-equivalent compositions ($\delta^{18}O_{olivine}$) at 1000 °C (Bindeman et al., 2005). These values are plotted in Fig. 5. Of 29 measurements on olivine and amphibole, 21 have $\delta^{18}O_{olivine}$ between 5.0 and 5.3, and so fall within the compositional range of MORB (Cooper et al., 2009). These include a mixture of olivine separates from basalts and amphibole separates from andesites

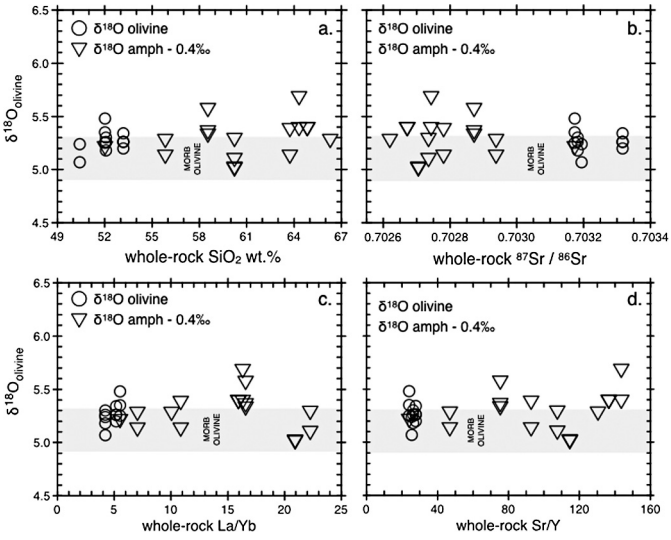

Fig. 5. Mineral oxygen isotope ratios ($\delta^{18}O_{olivine}$) in western Aleutian seafloor lavas versus whole-rock SiO_2 (a), $^{87}Sr/^{86}Sr$ (b), La/Yb (c) and Sr/Y (d). Oxygen isotope data are from Table 2. For amphibole samples the $\delta^{18}O_{olivine}$ is the measured $\delta^{18}O$ value form Table 2 minus 0.40‰ to produce an approximate olivine-equivalent composition (Bindeman et al., 2005). Whole-rock $^{87}Sr/^{86}Sr$ data are from Table 1. Other data are from Yogodzinski et al. (2015).

and dacites. The remaining 7 olivine and amphibole analyses have $\delta^{18}O_{olivine}$ from +5.4 to +5.7 (Table 2). The oxygen isotope data show no systematic change across widely variable whole-rock compositions for SiO_2, $^{87}Sr/^{86}Sr$, La/Yb or Sr/Y (Fig. 5).

Separates of other minerals from sample TN182-07-002 (Table 2) produced variable results with relatively high $\delta^{18}O$ in quartz (+9.5) and plagioclase (+7.0), but low $\delta^{18}O$ (+4.6) in clinopyroxene (Table 2). These variable $\delta^{18}O$ results and the presence of quartz xenocrysts indicate that sample TN182-07-002 is a hybrid or mixed rock that likely assimilated altered oceanic crust at

Table 2
Mineral oxygen and hydrogen isotope results.

Field ID	IGSN	Material[a]	$\delta^{18}O$ (‰) VSMOW[b]	δD (‰) VSMOW[b]	H_2O (wt.%)	Whole-rock SiO_2
TN182-09-001	GMY000041	olivine	5.07			50.4
TN182-09-001	GMY000041	olivine	5.24			50.4
TN182-07-002	GMY00003A	olivine	5.25			52.0
TN182-07-002	GMY00003A	olivine	5.48			52.0
TN182-07-002	GMY00003A	olivine	5.35			52.0
TN182-07-002	GMY00003A	amphibole	5.61			52.0
TN182-07-002	GMY00003A	quartz	9.53			52.0
TN182-07-002	GMY00003A	clinopyroxene	4.59			52.0
TN182-07-002	GMY00003A	plagioclase	6.97			52.0
TN182-08-014	GMY00003X	olivine	5.30			52.1
TN182-08-014	GMY00003X	olivine	5.26			52.1
TN182-08-014	GMY00003X	olivine	5.18			52.1
TN182-13-001	GMY00004L	olivine	5.20			53.2
TN182-13-001	GMY00004L	olivine	5.26			53.2
TN182-13-001	GMY00004L	olivine	5.34			53.2
TN182-13-001	GMY00004L	olivine	5.26			53.2
TN182-05-001	GMY000035	amphibole	5.68			55.8
TN182-05-001	GMY000035	amphibole	5.53			55.8
TN182-10-001	GMY000047	amphibole	5.97			58.5
TN182-10-001	GMY000047	amphibole	5.73			58.5
TN182-10-001	GMY000047	amphibole	5.76			58.5
TN182-11-005	GMY00004G	amphibole-1	5.42	−45.6	1.02	60.2
TN182-11-005	GMY00004G	amphibole-1	5.41			60.2
TN182-11-001	GMY00004C	amphibole	5.69	−77.0	1.19	60.2
TN182-11-001	GMY00004C	amphibole	5.50	−75.2	1.31	60.2
TN182-03-005	GMY00002Y	amphibole	5.78	−66.3	1.46	63.7
TN182-03-005	GMY00002Y	amphibole	5.53	−72.2	1.38	63.7
TN182-07-009	GMY00003H	amphibole	5.79	−45.8	1.59	64.3
TN182-07-009	GMY00003H	amphibole	6.08	−50.8	1.60	64.3
TN182-07-005	GMY00003D	amphibole	5.79	−46.4	1.58	64.9
TN182-07-005	GMY00003D	amphibole	5.59	−43.2	1.47	64.9
TN182-04-003	GMY000033	amphibole-1	5.68	−61.8	1.33	66.3

[a] Analyses of single crystals indicated by −1.
[b] Results of oxygen and hydrogen isotopes expressed relative Vienna Standard Mean Ocean Water on a permil (‰) basis.

shallow depths. Despite its complicated and apparently contaminated nature, olivine and amphibole separates from this sample fall within a narrow range ($\delta^{18}O_{olivine} = +5.2$ to $+5.4$) and are similar to olivine and amphibole from all other samples (Fig. 5). The origins of these MORB-like oxygen isotope compositions, which reflect the dominant source of the rocks, are discussed further below.

Hydrogen isotopes in amphibole separates (Table 2) encompass the nominal mantle range of −40 to −80‰ (Taylor and Sheppard, 1986) when correcting for ∼15‰ amphibole-melt fractionation (Tollan et al., 2012). Values for δD are generally higher in samples with higher amphibole H_2O (Table 2), but are not correlated with whole-rock isotope or trace element parameters.

5. Discussion

5.1. Expression of the eclogite melt component via Sr and $^{87}Sr/^{86}Sr$

We previously emphasized that high-Sr andesites and dacites among the western Aleutian seafloor lavas have characteristics expected in a geochemical source component produced by partial melting of MORB eclogite in the subducting oceanic crust (Yogodzinski et al., 2015). We also showed that this source component appears to be present in volcanic rocks throughout the Aleutian arc. In this context, an important aspect of these rocks, which has not been discussed, is the unradiogenic nature of their Sr and their high Sr abundances relative to other trace elements in comparisons to common Aleutian lavas and MORB.

In partial melts of MORB eclogite, Sr will fractionate from Ta, Nb, Y and heavy rare-earth elements (REEs), which partition into residual garnet and rutile. The incompatible behavior of Sr and relatively high abundance of Sr in MORB compared to mantle peridotite, also leads to the formation of Sr-rich magmas (Kay, 1978). As a result, plots of $^{87}Sr/^{86}Sr$ against Sr abundance, La/Ta, La/Yb, or Hf/Lu (Fig. 3) show strong inverse relationships for western seafloor lavas and in some cases, for all Aleutian volcanic rocks.

When all Aleutian data are considered, including samples from Piip Volcano, which are consistently offset toward mantle compositions in most plots of this type (Yogodzinski et al., 2015), the resulting data patterns (Fig. 3) are triangular in shape, with corners pointing toward subducted sediment and altered oceanic crust (upper-left), depleted mantle (lower-left) and eclogite melt (lower-right). Data patterns in these plots illustrate the point made in the introduction, that fluids and melts from altered oceanic crust and sediment cannot be the dominant source for Sr in Aleutian rocks. This point is most clearly illustrated in graphs of $^{87}Sr/^{86}Sr$ vs Y/Sr and Nd/Sr, where mixing lines are straight and plotted on an expanded scale to show sediment compositions at high $^{87}Sr/^{86}Sr$ (Figs. 6–7). It is evident from these plots that mixing of components from the depleted mantle, sediment and altered oceanic crust will generally produce compositions with $^{87}Sr/^{86}Sr$ greater than most Aleutian rocks. The patterns are unchanged if ratios with other light REEs are used on the horizontal scale (La/Sr, Ce/Sr, etc.). It is evident from these relationships that the Sr-rich and unradiogenic end-member in the Aleutian source must have Nd/Sr ∼0.01 and $^{86}Sr/^{86}Sr < 0.7029$. These are characteristics of the eclogite melt source component as expressed in high-Sr andesites and dacites from the western Aleutians. They are not the characteristics of fluids from altered oceanic crust (Figs. 6–7), which will commonly have $^{87}Sr/^{86}Sr$ from 0.7035 to 0.7050 (Staudigel, 2003 and references therein).

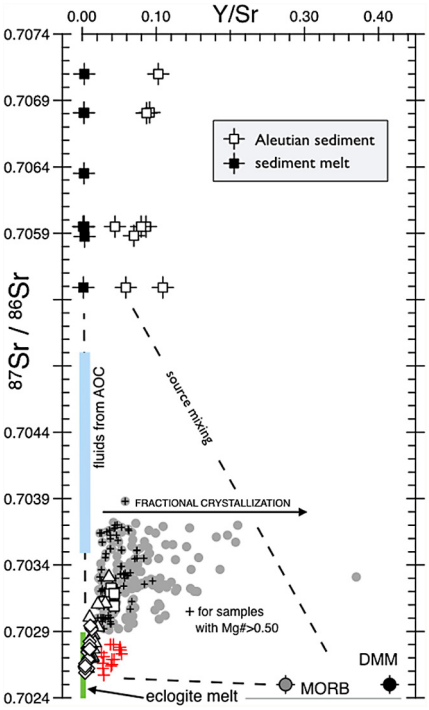

Fig. 6. Whole-rock $^{87}Sr/^{86}Sr$ in Aleutian volcanic rocks and sediment versus Y/Sr with source-mixing characteristics. Aleutian sediments are published data. Sediment melt Y–Sr ratios are model compositions (Yogodzinski et al., 2015) calculated from Aleutian sediment and using results of sediment-melting experiments (Hermann and Rubatto, 2009; Skora and Blundy, 2010). Fluids from altered oceanic crust (AOC – blue bar) are model compositions with Y/Sr < 0.02 calculated with 5–15% fluid extraction using partitioning data from experiments at 700° and 800 °C and 4 GPa by Kessel et al. (2005). The fluid source rock is seawater-altered basalt (Sr = 120, Y = 37.3 ppm) which is an average Pacific MORB from Gale et al. (2013) adjusted for seawater alteration using enrichment factors from the Site 801 super-composite of Kelley et al. (2003). Fluid $^{87}Sr/^{86}Sr$ values from 0.7035 to 0.7050 are similar to widely reported compositions for seawater-altered basalt (e.g., Alt et al., 1996; Staudigel, 2003). Eclogite melts (green bar) are model compositions with Y–Sr ratios <0.002 calculated as 5–10% melts with partitioning data from Kessel et al. (2005) at 900 °C and 4 GPa. The eclogite melt component has $^{87}Sr/^{86}Sr < 0.7029$ as expected for Pacific MORB + modest seawater alteration as discussed in the text. MORB and DMM and other data sources are as in Fig. 3. (For interpretation of the references to color in this figure legend, the reader is referred to the web version of this article.)

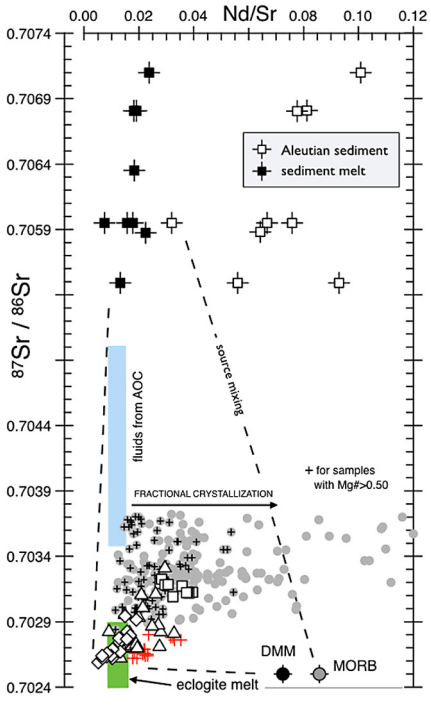

Fig. 7. Whole-rock $^{87}Sr/^{86}Sr$ in Aleutian volcanic rocks and sediment versus Nd/Sr with source-mixing characteristics. Fluids from altered oceanic crust (AOC – blue bar) are model compositions with 0.008 < Nd/Sr < 0.016 calculated with 5–15% fluid extraction using partitioning data from experiments at 700° and 800 °C and 4 GPa by Kessel et al. (2005). The fluid source rock is seawater-altered basalt (Sr = 120, Nd = 11.3 ppm) determined as in Fig. 7. Eclogite melts (green bar) are model compositions with 0.013 < Nd/Sr < 0.019 calculated as 5–10% melts with partitioning data from Kessel et al. (2005) at 900 °C and 4 GPa. Other data sources and modeling parameters are as in Fig. 6. (For interpretation of the references to color in this figure legend, the reader is referred to the web version of this article.)

A better trace element proxy for subduction fluids may be Ba/Th (George et al., 2003; Hawkesworth et al., 1997; Turner et al., 1996). However, Ba/Th has a narrow range in Aleutian rocks, from approximately 100 to 300 (Fig. 8). High concentrations of both elements appear to be linked to subducted sediment, so ratios such as Ba/La and Th/La are correlated with Pb and Sr isotopes and inversely correlated with ε_{Nd} (Kay and Kay, 1994; Kelemen et al., 2003b; Yogodzinski et al., 1994). As is the case in the Aleutians, Ba and Th concentrations are positively correlated in arc lavas worldwide (Fig. 12 in Kelemen et al., 2003a). Lavas with high Ba/Th have very low Ba and Th concentrations, whereas those with low Ba/Th have high concentrations of both elements. These important details are obscured by the use of element ratios only.

In a plot of $^{87}Sr/^{86}$ versus Ba/Th (Fig. 8), Aleutian lavas fall along binary mixing lines between MORB or depleted mantle and sediment. Thus, the $^{87}Sr/^{86}Sr$ versus Ba/Th plot fails to separate the eclogite melt and depleted mantle components and so cannot be used to quantify source characteristics. Something the $^{87}Sr/^{86}Sr$ versus Ba/Th plot does illustrate is that mixtures of depleted mantle with fluids from altered oceanic crust will generally have Ba/Th higher than Aleutian lavas (Fig. 8). Our main conclusion is that although some Ba/Th enrichment in Aleutian volcanic rocks from fluids derived from seawater-altered oceanic crust cannot be ruled out, the observed, correlated enrichments in both Ba and Th in Aleutian rocks must come predominantly from a subducted sediment component (Kay and Kay, 1994; Kelemen et al., 2003b; Plank, 2005; Yogodzinski et al., 1994).

The strong inverse correlation between Nd and Sr isotope ratios observed in Aleutian volcanic rocks (Fig. 9) reinforces the point that subducted sediment contributes significant Sr and Nd to the Aleutian source (Class et al., 2000; Kay, 1980; Plank, 2005), and that the dominant mixing is between sediment and one or more depleted end-member(s) with $^{87}Sr/^{86}Sr < 0.703$. Again, in Fig. 9 as in many isotope–isotope plots, we infer that there must be two source components at the depleted end of the mixing array (Yogodzinski et al., 2015). One is the eclogite melt component, which has high Sr/Nd and produces strongly curved mixing lines with sediment. The other is the depleted mantle, which has Sr/Nd similar to bulk sediment, and so produces straight mixing lines. The two end-member mixing lines encompass the data field for Aleutian volcanic rocks (Fig. 9).

Thus, the combined data patterns in Figs. 7–9 indicate that aqueous fluids from altered oceanic crust cannot be a dominant contributor of Sr to the source of Aleutian volcanic rocks. These results also imply that in Aleutian rocks, the dominant source of unradiogenic subducted Sr may be produced by melting of MORB eclogite in the subducting plate (i.e., it is the eclogite-melt source component – Yogodzinski et al., 2015). Moreover, the combination of high Sr and unradiogenic Sr isotopes is observed in arc volcanic rocks globally (Hawkesworth et al., 1993).

Basic modeling results indicate that much of the fractionation of Sr from Nd concentrations observed in high-Sr, western Aleutian dacites (Nd/Sr ~ 0.01) compared to MORB (Nd/Sr ~ 0.09) is produced by residual garnet. Using bulk solid/liquid partition coefficients from the Kessel et al. (2005) experiments at 900 °C and

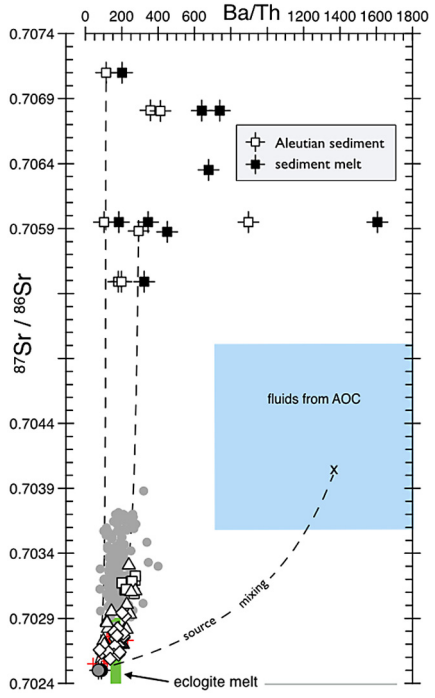

Fig. 8. Whole-rock $^{87}Sr/^{86}Sr$ in Aleutian volcanic rocks and sediment versus Ba/Th with source-mixing characteristics. Mixtures with depleted MORB mantle use values from Salters and Stracke (2003). Fluids from altered oceanic crust (AOC – blue bar) are model compositions extracted from seawater-altered basalt (Ba = 24, Th = 0.34 ppm) determined as in Fig. 6. Mixing end-member 'x' is a 5% fluid at 800 °C with 208 ppm Ba and 0.513 ppm Th. The total range for Ba/Th in the AOC fluids is 710–2807 based on 5–15% fluid extraction. The sediment mixing end-members are turbidites from DSDP178 (Ba/Th = 232, Th = 4.38 ppm) and DSDP183 (Ba/Th = 112, Th = 6.63). Eclogite melts (green bar) are model compositions with Ba/Th calculated as 5–10% melts using partitioning data from Kessel et al. (2005) at 900° and 4 GPa. Other data sources and modeling parameters are as in Fig. 6. (For interpretation of the references to color in this figure legend, the reader is referred to the web version of this article.)

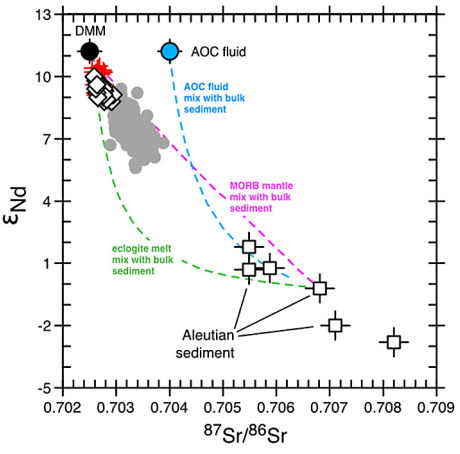

Fig. 9. Whole-rock ε_{Nd} versus $^{87}Sr/^{86}Sr$ in Aleutian volcanic rocks and sediment with source-mixing characteristics. Dashed lines are mixtures with an average bulk sediment composition with Sr = 235 ppm, Nd = 19.0 ppm, $^{87}Sr/^{86}Sr = 0.7068$, and $\varepsilon_{Nd} = -0.2$. The depleted mantle mixing end-member has Nd and Sr concentrations from Salters and Stracke (2003) with $^{87}Sr/^{86}Sr = 0.7025$ and $\varepsilon_{Nd} = 11.2$, similar to northeast Pacific MORB (Gale et al., 2013). The eclogite melt end-member is an average western Aleutian dacite with Sr = 1470 ppm, Nd = 11.5 ppm, $^{87}Sr/^{86}Sr = 0.70262$ and $\varepsilon_{Nd} = 9.5$ (Yogodzinski et al., 2015). The AOC fluid mixing end-member is a model composition with Sr = 42.2 ppm and Nd = 0.652 ppm, based on a 5% fluid and partitioning from 4 GPa experiments at 800 °C from Kessel et al. (2005). The fluid has $^{87}Sr/^{86}Sr = 0.7040$ based on typical seawater-altered basalt and $\varepsilon_{Nd} = 11.2$ like northeast Pacific MORB (Gale et al., 2013). Other data sources and modeling parameters are as in Fig. 6.

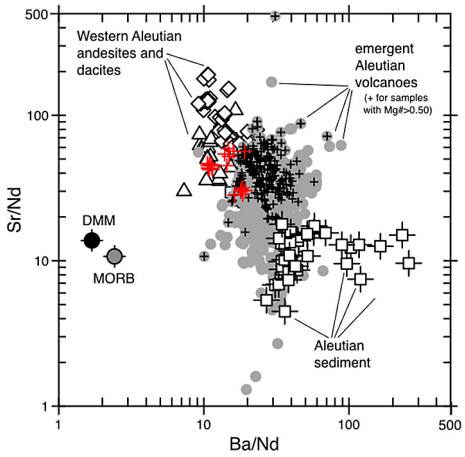

Fig. 10. Whole-rock Sr/Nd versus Ba/Nd in Aleutian volcanic rocks and sediments compared to MORB and depleted MORB mantle (DMM). Symbols and data sources are as in Figs. 2 and 9.

4 GPa ($D_{Sr} = 0.047$, $D_{Nd} = 0.662$), a 5% batch melt of Pacific MORB with Sr ~128 ppm and Nd/Sr ~0.095 (Gale et al., 2013), will have 1347 ppm Sr and Nd/Sr of 0.013. Kessel et al. (2005) report that garnets in this experiment had Nd/Sr = 69.6 (Nd = 41 ± 6 ppm, Sr = 0.60 ± 0.2 ppm) and so likely account for most of the fractionation of Nd/Sr from ~0.09 in the MORB eclogite source to ~0.01 in the eclogite melt. Partitioning from experiments at 1000 °C and 4 GPa (Kessel et al., 2005) produce eclogite melts with similar Sr abundances and slightly higher Nd/Sr (Sr = 1371 ppm, Nd/Sr = 0.026). Thus, fluids from altered oceanic crust and melts of MORB eclogite produce similar fractionation of Sr from Nd (Fig. 7), but not Ba from Th (Fig. 8). More broadly, the decoupling of Ba and Sr enrichments from Nd (Fig. 10) indicates that aqueous fluid enrichment is not a significant factor in controlling Ba and Sr budgets in Aleutian rocks (see also figure 12 in Kelemen et al., 2003a). Again, enrichments in Ba are linked primarily to a subducted sediment in Aleutian rocks (Fig. 8) and appear unrelated to enrichments in Sr which are linked to the eclogite melt component and appear to be controlled by residual garnet (Fig. 10).

5.2. Subducted serpentinite as a source of H_2O and Sr

The unradiogenic nature of Sr in western Aleutian andesite and dacite ($^{87}Sr/^{86}Sr < 0.7027$) is perhaps surprising, given our interpretation that these lavas contain a substantial component derived by hydrous partial melting of subducted basalt, which should carry relatively radiogenic Sr, due to effects of seawater alteration. This is an acute problem for the end-member western Aleutian samples, because their Sr concentrations are high (Sr > 1000 ppm) and because petrographic observations indicate that they are H_2O-rich (Yogodzinski et al., 2015).

Fluids held in micas and amphiboles and other hydrous minerals in seawater-altered MORB could drive in-situ, fluid-absent melting within subducting oceanic crust (e.g., Beard and Lofgren, 1991). However, H_2O in hydrous minerals in such a source was derived from seawater, and will commonly contain radiogenic Sr with $^{87}Sr/^{86}Sr$ ~0.704 (Staudigel, 2003). Fluid-absent melting of such a source cannot contribute significantly to the formation of western Aleutian high-Sr dacites, which have $^{87}Sr/^{86}Sr$ ~0.7026 (Fig. 3a). Assuming that potential sources of H_2O lie primarily in subducting sediment and AOC (which contain radiogenic Sr), it is evident from the unradiogenic nature of Sr in western Aleutian andesites and dacites that the H_2O they contain cannot have been transported in fluids that contributed significantly to their Sr budgets.

One source of H_2O with low Sr is partially serpentinized peridotite within the mantle section of the subducting plate, which

may be formed in ocean ridge hydrothermal systems and by seawater ingress along normal faults formed as the subducting plate passes over the outer rise and descends into the trench (Peacock, 2001; Ranero et al., 2003). Serpentine formed in the cool interior of the subducting plate may be transported to its maximum pressure stability of ~7 GPa, which extends beyond subarc depths (Ulmer and Trommsdorff, 1995). As the subducting plate descends, an inverted geothermal gradient of >200–300 °C is established, so the top of the plate may be heated to temperatures required for fluid-saturated melting (700–750 °C at 3 GPa), at approximately the point where serpentinite dehydration creates fluid release from the plate's interior. This creates a situation where melting of basaltic crust within the subducting plate can be fluxed by fluids produced by dehydration of the underlying serpentine (Poli and Schmidt, 2002; Portnyagin et al., 2007; Walowski et al., 2015).

Partially serpentinized mantle peridotites have a range of Sr concentration and $^{87}Sr/^{86}Sr$, depending on water/rock ratios in the systems that lead to serpentinization. We assume the worst case for our purposes, which is that Sr carried in fluids from dewatered serpentinite beneath the Aleutian arc has the isotopic composition of modern seawater ($^{87}Sr/^{86}Sr = 0.709$). With this starting point, the two things needed to calculate a mass balance for the source of Aleutian Sr are (1) the Sr abundance in the serpentinite that is the source of the fluid and (2) the Sr abundance in the aqueous fluid produced by dehydration of that serpentinite.

Serpentinized abyssal peridotites are formed predominantly by the interaction of seawater with depleted peridotite and so provide a reasonable estimate for serpentinite formed within the subducting plate and entering the Aleutian subduction zone. In data for 84 abyssal peridotites compiled by Deschamps et al. (2013), the average Sr abundance is aliased by 9 samples with >100 ppm Sr, including three with >1000 ppm Sr. Of the remaining 75 analyses, 72 contain <10 ppm Sr. If the 9 anomalous samples are excluded, the mean Sr abundance in the filtered dataset is 3.5 ppm ± 6.3 (1σ). Based on these values, it is reasonable to infer that serpentinite within the subducting plate as it enters the Aleutian subduction zone will not generally contain more than ~16 ppm Sr (the average plus two standard deviations).

Experimental studies provide a basis for estimating Sr abundances in fluids produced by dehydration of serpentinite. Tatsumi et al. (1986) found that 10 to 19% of Sr was extracted from serpentinite during dehydration, which was measurably less than the 17–25% extraction of La. Tenthorey and Hermann (2004) found that fluids produced by serpentine dehydration in diamond trap experiments never had higher Sr than their starting material, and in this respect, their results for Sr were similar to those for Ce. Concentrations of Sr in fluids derived by serpentine dehydration at 3.5 GPa were 1.6 to 1.8 – times higher than in the starting serpentinite composition (Spandler et al., 2014) and similar to fluid/rock partitioning of Ce (3.0–3.8) and less than for Cs (10–16) and Pb (8.6–9.4). Thus, experimental results indicate that Sr concentrations in fluids produced by dehydrating serpentinite will not be more than a factor of ~2 greater than Sr concentrations in the source. Thus, fluids produced by dehydration of serpentinized peridotite with less than 16 ppm Sr should contain no more than 32 ppm Sr. This estimate is similar to Sr abundances of 20–30 ppm measured in fluid inclusions in olivine–orthopyroxene–chlorite rocks produced by prograde metamorphism of serpentinite at subduction depths (Scambelluri et al., 2004).

Assuming that 2% H_2O is sufficient to drive significant melting of MORB eclogite (e.g., Schmidt et al., 2004), the addition of seawater Sr in the fluid ($^{87}Sr/^{86}Sr = 0.709$) to Pacific MORB eclogite ($^{87}Sr/^{86}Sr = 0.70255$) will raise $^{87}Sr/^{86}Sr$ in the mixture over fresh MORB by only 0.00003 to 0.00005, for 80 to 130 ppm Sr in eclogite. In other words, if Pacific MORB eclogite has 80–130 ppm Sr and $^{87}Sr/^{86}Sr = 0.70255$, the addition of 2% of fluid with 32 ppm Sr and $^{87}Sr/^{86}Sr = 0.709$ will produce rock–fluid mixtures with $^{87}Sr/^{86}Sr$ from 0.70258 to 0.70260. This mass balance indicates that fluids produced by dehydration of serpentinite in the mantle section of the subducting Pacific Plate will carry little Sr and have minimal impact on the isotopic composition of the source mixture if MORB eclogite with 80–130 ppm Sr is the dominant source of the melt.

This simple model provides a mechanism by which high-Sr dacites from the western Aleutians, which have $^{87}Sr/^{86}Sr \sim 0.7026$, may represent the end-member eclogite-melt source component for Sr, as they do for Pb, Nd and Hf (Yogodzinski et al., 2015). It must also be true that the source of the high-Sr dacites does not contain a significant quantity of subducted sediment, and that the bulk of the MORB eclogite source in the subducting plate cannot have been greatly affected by seawater alteration. These points are discussed further below. An important additional result of this model is that it decouples the dominant source of H_2O, derived by dehydration of subducting serpentine, from the dominant source of incompatible trace elements, produced via partial melting of subducted sediment and basalt. This decoupling of H_2O and trace element sources is also suggested by the observation of widely variable trace element abundances compared to more restricted variability for H_2O inferred from least-degassed melt inclusions in the global arc database (Plank et al., 2013; Portnyagin et al., 2007).

5.3. Subducted oceanic crust as a source of Sr

The end-member character of western Aleutian andesites and dacites in many isotope-trace element ratio plots (Figs. 3 and 6–9) is a reflection of their isotopically depleted compositions ($^{87}Sr/^{86}Sr \sim 0.7026$) combined with Sr-rich (Nd/Sr ~ 0.01) and fractionated trace element patterns. These are distinctive characteristics compared to common arc lavas but they are not unique globally, or even uncommon. In fact, we see qualitatively similar shifts from common arc-basalt/andesite compositions toward less radiogenic Sr and higher Sr abundances in high Sr/Nd andesites and dacites in many Circum-Pacific locations, including Baja California (Rogers et al., 1985), Patagonia (Stern and Killian, 1996; Kay et al., 1993), Solander Island, New Zealand (Foley et al., 2012), the Solomon Islands (König et al., 2007), Antarctica (McCarron and Smellie, 1998), the southern-most Cascade arc (Grove et al., 2002; Walowski et al., 2015) and other parts of northern California (Johnson and O'Neil, 1984). In all of these locations, subducting lithosphere is young (Defant and Drummond, 1990) and/or associated with a slab window or oblique convergence, where plate edges may be exposed to heating by mantle flow on three sides (Yogodzinski et al., 2001). Thus, it is a hot-slab setting and a distinctive geochemical pattern that unites these locations. Assuming that the geochemical pattern reflects a relatively large source component produced by melting of the basaltic part of the subducting plate under eclogite conditions (Defant and Drummond, 1990; Kay, 1978), the observed shift toward relatively unradiogenic Sr means that in the places where the effects of eclogite melting are most evident, the melting process commonly encompasses a significant portion of oceanic crust that was not subject to prior effects of seawater alteration.

Oceanic crustal sections in ophiolites commonly exhibit extensive effects of seawater alteration with $^{87}Sr/^{86}Sr > 0.704$ throughout the sheeted dikes and into the upper gabbros at depths of 2–3 km (e.g., Bickle and Teagle, 1992). If it were subducted, this part of an oceanic crustal section could not be the source of Sr in end-member western Aleutian dacites, which have $^{87}Sr/^{86}Sr$ ~0.7026 (Fig. 3a). More broadly, such extensively altered oceanic crust cannot be the source of Sr in Aleutian lavas in general

because mixtures of source components from Aleutian sediment ($^{87}Sr/^{86}Sr$ ~0.706), seawater-altered basalt ($^{87}Sr/^{86}Sr$ >0.704), and depleted Pacific mantle ($^{87}Sr/^{86}Sr$ ~0.7025), do not encompass the compositions of Aleutian lavas in $^{87}Sr/^{86}Sr$ vs Nd/Sr space (Fig. 7) or in other similar plots involving Sr isotopes.

Ocean drilling provides samples of oceanic crust that are less extensively affected by seawater alteration (Davis et al., 2003) and so provide a more plausible subducted source for Aleutian Sr. At Site 504B (eastern equatorial Pacific), where drilling penetrated 1800 m into oceanic basement, the average $^{87}Sr/^{86}Sr$ of all samples in the sheeted dike section is 0.7029 (Alt et al., 1996; Bach et al., 2003), which is little different from fresh MORB from the Galapagos Ridge (the source of oceanic lithosphere at Site 504B), which have $^{87}Sr/^{86}Sr = 0.7028 \pm 0.0002$ ($n = 93$, Gale et al., 2013). Höfig et al. (2014) similarly showed at nearby Site 1256, that significant seawater alteration effects on $^{87}Sr/^{86}Sr$ were concentrated in the lower volcanic section and upper sheeted dikes, with most samples at lower stratigraphic positions falling within or close to the range of $^{87}Sr/^{86}Sr$ observed in fresh MORB at the site. Data compiled from the MARK and Atlantis II Fracture Zone areas also show modest effects of seawater alteration on $^{87}Sr/^{86}Sr$ at depths of 1.5–2.0 km into oceanic basement (Davis et al., 2003).

Thus, the unradiogenic nature of Sr in Aleutian rocks overall ($^{87}Sr/^{86}Sr < 0.7036$), and in end-member western Aleutian samples in particular (Figs. 3 and 6–9), means that melting of the subducting plate cannot be confined to the volcanic section (near the top of the plate), where seawater alteration is often extensive (Alt et al., 1996; Höfig et al., 2014; Staudigel, 2003). Instead, if the eclogite melt component is the dominant source of Aleutian Sr, then eclogite melting beneath the Aleutian arc must extend down to minimally altered parts of the sheeted dike section, more than 2 km below the paleo-seafloor in the subducting plate. An additional effect may be that extensive dehydration of seawater altered basalt at the top of the slab (as predicted by thermal models – Syracuse and Abers, 2006; van Keken et al., 2011) may commonly remove a significant proportion of radiogenic Sr at relatively shallow depths beneath the forearc and prior to eclogite melting. If so, melts produced from the upper volcanic section at greater depths would contain less radiogenic Sr than expected from seawater-altered basalt with $^{87}Sr/^{86}Sr > 0.7040$ (Staudigel, 2003). This could contribute to an eclogite melt component with low Nd/Sr and relatively unradiogenic Sr as required by mass balance (Figs. 7–10).

Finally, oxygen isotope ratios in western Aleutian lavas (Fig. 5) are similar to fresh MORB and mantle values (Cooper et al., 2009). These data are inconsistent with melting confined to highly altered seafloor volcanic rocks, in which relatively high $^{18}O/^{16}O$ ratios are observed (Alt et al., 1996; Staudigel, 2003). Based on oxygen isotope stratigraphy at Site 504B (Alt et al., 1996), melting to the base of the sheeted dikes would encompass a significant proportion of oceanic crust with isotopically light oxygen ($\delta^{18}O < 4‰$) that would offset (in a mass-balance sense) isotopically heavy oxygen derived from highly altered lavas, and thereby create an eclogite melt component with MORB and mantle-like oxygen isotope ratios, as seen in western Aleutian lavas ($\delta^{18}O = 5.1–5.7$, Fig. 5). This would achieve the effects of "whole-slab melting", as discussed by Bindeman et al. (2005), though it should be noted that interaction of eclogite melts with mantle peridotite as they rise to the surface may also contribute to the MORB-like and mantle oxygen isotopes values in western Aleutian seafloor lavas (Fig. 5).

5.4. Reconciling Aleutian Sr with thermal models

Melting of subducting oceanic crust will occur where sufficient water is present and when temperatures exceed the fluid-saturated solidus of MORB eclogite. The presence of these conditions in a subduction zone depend on the thermal structure of the subducting plate, as reflected in the thermal parameter (Φ), which is the product of slab age and the orthogonal subduction rate (Kirby et al., 1991). Excluding the anomalously cold Tonga slab ($\Phi > 14{,}000$), thermal parameters vary globally from 100–400 in hot-slab systems such as the Cascades and Mexico, to 6000–7000 in cold-slab systems such as the Kuriles and South Mariana arc (Syracuse and Abers, 2006). The average thermal parameter for three Aleutian locations ($\Phi = 2577$, $1\sigma = 247$) is above the median for all arcs ($\Phi = 2095$) but below the coolest ~30% which have $\Phi > 4000$ (Syracuse and Abers, 2006). So, the Aleutians may be considered a moderate-to-cool arc. At subarc depths around 100 km (3.0 to 3.5 GPa), an ensemble of thermal models yield Aleutian slab-top temperatures consistently above the fluid-saturated solidus for MORB eclogite at 700–800 °C (Syracuse et al., 2010). In turn, these model estimates are somewhat cooler than those from geochemical proxies such as Ce/H_2O, which place Aleutian slab-top temperatures ~830 °C (Cooper et al., 2012; Plank et al., 2009). At the bottom of the sheeted dikes in the subducting plate, which will commonly lie 2 km below paleo-seafloor, temperatures are expected to be significantly cooler. Modeling results for the southern Mariana arc ($\Phi = 6350$) and temperature variation within the crustal sections of subducting plates globally indicate that temperatures several km below the top of subducting oceanic crust beneath the Aleutian arc should be more than 100 °C below the temperature at the top of the subducting plate (see figures 2 and 4b in van Keken et al., 2011).

Modeling results thus indicate that in the presence of sufficient water, melting of sediment and basalt at the top of the subducting oceanic plate beneath the Aleutians is possible, but that – if the subducting oceanic plate is intact – melting should not extend to the base of the sheeted dike section, as our analysis of geochemical data seems to require. An additional point is that dehydration of sediment and seawater altered basalt at the top of the subducting plate beneath the forearc (e.g., Syracuse et al., 2010; van Keken et al., 2011) is also likely to limit melt production even in the hottest part of the slab. Thus, subduction zone thermal models appear to be at odds with Aleutian geochemical data presented here.

There are several possible ways to resolve this apparent discrepancy. Subducting plates may commonly be buckled and torn (Yamaoka et al., 1986), or intensely sheared and broken at the plate interface and thus exposed to heating in ways that are not captured by two-dimensional thermal models (e.g., Bebout and Penniston-Dorland, 2016; Penniston-Dorland et al., 2015). Heating of subducting lithosphere from below may also be a greater effect than is appreciated. For example, Hawley et al. (2016) observe a low-velocity seismic anomaly beneath the outer rise portion of the subducting Juan de Fuca plate along the full length of the Cascadia subduction zone. If this anomaly is in fact a 900 km-long cylinder of partial melt (Hawley et al., 2016) it implies the advection of heat to the base of the subducting plate which may effect the thermal structure of the plate's interior as it passes beneath the trench and forearc and enters the subduction zone. It may also be that subducting sediments and altered lavas are commonly transferred from the footwall into the hanging wall along imbricate thrust faults and shear zones. A variety of studies have also concluded that sedimentary sections at the top of subducting plates may be physically separated from the underlying basaltic oceanic crust by density instabilities leading to diapirs (Behn et al., 2011; Gerya and Yuen, 2003; Kelemen et al., 2003a; Marschall and Schumacher, 2012). Evidence that this process has occurred may be found in the highly depleted isotopic compositions of most seafloor volcanic rocks west of Buldir Island, which indicate the geochemical influence of subducted sediment there is nearly zero (Kelemen et al., 2003b; Yogodzinski et al., 2015, 1994; Nielsen et al., 2016). Such depleted compositions are most easily explained if the sedimentary section and perhaps the sheared and

hydrated portions of the uppermost volcanic section (the mélange – Marschall and Schumacher, 2012) were physically separated from the top of the subducting plate. If the sedimentary section were incorporated into the mantle wedge by diapirs (Behn et al., 2011; Gerya and Yuen, 2003; Kelemen et al., 2003a; Marschall and Schumacher, 2012), then increasingly oblique subduction along the arc and weak coupling at the top of the slab could cause the subducting plate to effectively outrun the overlying column of mantle rock so that in the westernmost parts of the arc, partial melts from the basaltic part of the slab would rise in a mantle wedge that had not been contaminated by sediment diapirs.

6. Conclusions

Results of this study reinforce the conclusion that high Mg# andesites and dacites from seafloor volcanoes in the western Aleutians exhibit trace element and isotopic characteristics produced by melting of MORB eclogite in oceanic crust of the subducting Pacific Plate. Mixing relationships in plots of $^{87}Sr/^{86}Sr$ versus Nd/Sr and ε_{Nd} versus $^{87}Sr/^{86}Sr$ rule out aqueous fluids as a significant source for Sr in Aleutian rocks. Water required to drive eclogite melting in the oceanic crust is likely produced by serpentine breakdown in the underlying mantle section of the subducting plate. Fluids produced by serpentine breakdown will carry little Sr and have minimal impact on $^{87}Sr/^{86}Sr$ in the source mixture. MORB-like Sr and O isotopes in end-member samples indicate that eclogite melting must encompass a bulk composition that has been little-affected by seawater alteration. Eclogite melting must consequently extend to depths of 2+ km into the subducting plate. These findings imply that subducting lithosphere beneath the Aleutian arc is significantly hotter than indicated by thermal models.

Acknowledgements

The authors thank E. Bair, C. Frisby, S. Henrick and M. Siegrist for their assistance with data collection at the University of South Carolina, and to J. Blusztajn for his assistance at Woods Hole. Thanks also to G. Hart and C. Knaack for technical help at the ICP-MS facility at Washington State University. The cooperation of SM Kay and RW Kay is gratefully acknowledged. Thanks also go to T. Murray, T. Miller, M. Coombs, J. Power and others at the USGS and Alaska Volcano Observatory for their generous support. Support for STB during manuscript preparation was provided by the Director, Office of Science, Office of Basic Energy Sciences, of the U.S. Department of Energy under Contract No. DE-AC02-05CH11231. This paper benefited from the helpful comments of Richard Arculus, an anonymous reviewer, and editor Mike Bickle.

Funding

This work was supported by US National Science Foundation Grants EAR-0230261 to JDV; EAR-0510671 to KWWS; EAR-1447337 to IB; EAR-0509922, EAR-0236481, OCE-0242585 and OCE-0728077 to GMY; OCE-0242233, OCE-0533226, OCE-1144759, EAR-0727013, EAR-0961359 and EAR-0742368 to PBK. This work was also supported by the German Ministry for Education and Research for R/V SONNE cruises SO201-1b and SO249-1 (BMBF; Grants 03G0201A KALMAR and 03G0249 BERING).

References

Alt, J.C., Teagle, D.A.H., Bach, W., Halliday, A.N., Erzinger, J., 1996. Stable and strontium isotopic profiles through hydrothermally altered upper oceanic crust, Hole 504B. In: Alt, J.C., Kinoshita, H., Stokking, L.B., Michael, P.J. (Eds.), Proceedings of the Ocean Drilling Program, Scientific Results, vol. 148. Ocean Drilling Program, College Station, pp. 57–69.

Bach, W., Peucker-Ehrenbrink, B., Hart, S.R., Blusztain, J., 2003. Geochemistry of hydrothermally altered oceanic crust: DDP/ODP Hole 504B – implications for seawater–crust exchange budgets and Sr- and Pb-isotopic evolution of the mantle. Geochem. Geophys. Geosyst. 4.

Beard, J.S., Lofgren, G.E., 1991. Dehydration melting and water-saturated melting of basaltic and andesitic greenstones and amphibolites at 1, 3, and 6–9 kb. J. Petrol. 32, 365–401.

Bebout, G.E., Penniston-Dorland, S.C., 2016. Fluid and mass transfer at subduction interfaces – the field metamorphic record. Lithos 240–243, 228–258.

Behn, M.D., Kelemen, P.B., Hirth, G., Hacker, B.R., Massonne, H.J., 2011. Diapirs as the source of the sediment signature in arc lavas. Nat. Geosci. 4, 641–646.

Bickle, M.J., Teagle, D.A.H., 1992. Strontium alteration in the Troodos ophiolite: implication for fluid fluxes and geochemical transport in mid-ocean ridge hydrothermal systems. Earth Planet. Sci. Lett. 113, 219–237.

Bindeman, I.N., Eiler, J.M., Yogodzinski, G.M., Tatsumi, Y., Stern, C.R., Grove, T.L., Portnyagin, M., Hoernle, K., Danushevsky, L.V., 2005. Oxygen isotope evidence for slab melting in modern and ancient subduction zones. Earth Planet. Sci. Lett. 235, 480–496.

Bindeman, I.N., Kamenetsky, V.S., Palandri, J., Vennemann, T., 2012. Hydrogen and oxygen isotope behavior during variable degrees of upper mantle melting: example from the basaltic glasses from Macquarie Island. Chem. Geol. 310–311, 126–136.

Class, C., Miller, D.M., Goldstein, S.L., Langmuir, C.H., 2000. Distinguishing melt and fluid subduction components in Umnak Volcanics, Aleutian Arc. Geochem. Geophys. Geosyst. 1.

Cooper, K.M., Eiler, J.M., Sims, K.W.W., Langmuir, C.H., 2009. Distribution of recycled crust within the upper mantle: insights from the oxygen isotope composition of MORB from the Australian–Antarctic discordance. Geochem. Geophys. Geosyst. 10.

Cooper, L.B., Ruscitto, D.M., Plank, T., Wallace, P.J., Syracuse, E.M., Manning, C.E., 2012. Global variations in H_2O/Ce: 1. Slab surface temperatures beneath volcanic arcs. Geochem. Geophys. Geosyst. 13.

Davis, A.C., Bickle, M.J., Teagle, D.A.H., 2003. Imbalance in the oceanic strontium budget. Earth Planet. Sci. Lett. 211, 173–187.

Defant, M.J., Drummond, M.S., 1990. Derivation of some modern arc magmas by melting of young subducted lithosphere. Nature 347, 662–665.

Deschamps, F., Godard, M., Guillot, S., Hattori, K., 2013. Geochemistry of subduction zone serpentinites: a review. Lithos 178, 96–127.

Foley, F.V., Pearson, N.J., Rushmer, T., Turner, S., Adam, J., 2012. Magmatic evolution and magma mixing of quaternary adakites at Solander and Little Solander Islands, New Zealand. J. Petrol. 54, 703–744.

Gale, A., Dalton, C.A., Langmuir, C., Su, Y., Schilling, J.G., 2013. The mean composition of ocean ridge basalt. Geochem. Geophys. Geosyst. 14.

George, R., Turner, S., Hawkesworth, C.J., Morris, J., Nye, C., Ryan, J.G., Zheng, S.-H., 2003. Melting processes and fluid and sediment transport rates along the Alaska–Aleutian arc from an integrated U–Th–Ra–Be isotope study. J. Geophys. Res., Solid Earth 108, 1–25.

Gerya, T.V., Yuen, D.A., 2003. Rayleigh–Taylor instabilities from hydration and melting propel 'cold plumes' at subduction zones. Earth Planet. Sci. Lett. 212, 47–62.

Grove, T., Parman, S.W., Bowring, S.A., Price, R., Baker, M.B., 2002. The role of an H_2O-rich fluid component in the generation of primitive basaltic andesites and andesites from the Mt. Shasta region, N California. Contrib. Mineral. Petrol. 142, 375–396.

Hawkesworth, C., O'Nions, R.K., Arculus, R.J., 1979. Nd and Sr isotope geochemistry of island arc volcanics, Grenada, Lesser Antilles. Earth Planet. Sci. Lett. 45, 237–248.

Hawkesworth, C.J., Hergt, J.M., Ellam, R.M., McDermott, F., 1991. Element fluxes associated with subduction related magmatism. Philos. Trans. R. Soc. Lond. 335, 393–405.

Hawkesworth, C.J., Gallagher, K., Hergt, J.M., McDermott, F., 1993. Mantle and slab contributions in arc magmas. Annu. Rev. Earth Planet. Sci. 21, 175–204.

Hawkesworth, C.J., Turner, S.P., McDermott, F., Peate, D.W., van Calsteren, P., 1997. U–Th isotopes in arc magmas: implications for element transfer from the subducted crust. Science 276, 551–555.

Hawley, W.B., Allen, R.M., Richards, M.A., 2016. Tomography reveals buoyant asthenosphere accumulating beneath the Juan de Fuca plate. Science 353, 1406–1408.

Hermann, J., Rubatto, D., 2009. Accessory phase control on the trace element signature of sediment melts in subduction zones. Chem. Geol. 265, 512–526.

Hildreth, W., Fierstein, J., 2000. Katmai volcanic cluster and the great eruption of 1912. Geol. Soc. Am. Bull. 112, 1594–1620.

Höfig, T.W., Geldmacher, J., Hoernle, K., Hauff, F., Duggen, S., Garbe-Schönberg, D., 2014. From the lavas to the gabbros: 1.25 km of geochemical characterization of upper oceanic crust at ODP/IODP Site 1256, eastern equatorial Pacific. Lithos 210–211, 289–312.

Johnson, C.M., O'Neil, J.R., 1984. Triple junction magmatism: a geochemical study of Neogene volcanic rocks in western California. Earth Planet. Sci. Lett. 71, 241–262.

Kay, R.W., 1978. Aleutian magnesian andesites: melts from subducted Pacific Ocean crust. J. Volcanol. Geotherm. Res. 4, 117–132.

Kay, R.W., 1980. Volcanic arc magma genesis: implications for element recycling in the crust–upper mantle system. J. Geol. 88, 497–522.
Kay, S.M., Kay, R.W., 1994. Aleutian magmas in space and time. In: Plafker, G., Berg, H.C. (Eds.), The Geology of Alaska. Geological Society of America, Boulder, pp. 687–722.
Kay, S.M., Ramos, V.A., Marquez, Y.M., 1993. Evidence in Cerro Pampa volcanic rocks for slab-melting prior to ridge-trench collision in southern South America. J. Geol. 101, 703–714.
Kelemen, P.B., Hanghøj, K., Greene, A.R., 2003a. One view of the geochemistry of subduction-related magmatic arcs, with an emphasis on primitive andesite and lower crust. In: Holland, H.D., Turekian, K.K. (Eds.), Treatise on Geochemistry. Elsevier, New York, pp. 593–659.
Kelemen, P.B., Yogodzinski, G.M., Scholl, D.W., 2003b. Along-strike variation in lavas of the Aleutian Island Arc: implications for the genesis of high Mg# andesite and the continental crust. In: Eiler, J. (Ed.), Inside the Subduction Factory. In: Geophys. Monogr., vol. 138. American Geophysical Union, Washington, DC, pp. 223–276.
Kelley, K.A., Plank, T., Ludden, J.N., Staudigel, H., 2003. Composition of altered oceanic crust at ODP Sites 801 and 1149. Geochem. Geophys. Geosyst. 4, 21.
Kessel, R., Schmidt, M.W., Ulmer, P., Pettke, T., 2005. Trace element signature of subduction-zone fluids, melts and supercritical liquids at 120–180 km depth. Nature 437, 724–727.
Kirby, S.H., Durham, W.B., Stern, L.A., 1991. Mantle phase changes and deep-earthquake faulting in subducted lithosphere. Science 252, 216–225.
König, S., Schuth, S., Münker, C., Qopoto, C., 2007. The role of slab melting in the petrogenesis of high-Mg andesites: evidence from Simbo Volcano, Solomon Islands. Contrib. Mineral. Petrol. 153, 85–103.
Lacasse, C., Sigurdsson, H., Carey, S.N., Jóhannesson, H., Thomas, L.E., Rogers, N.W., 2007. Bimodal volcanism at the Katla subglacial caldera, Iceland: insight into the geochemistry and petrogenesis of rhyolitic magmas. Bull. Volcanol. 69, 373–399.
Marschall, H.R., Schumacher, J.C., 2012. Arc magmas sourced from mélange diapirs in subduction zones. Nat. Geosci. 5, 862–867.
McCarron, J.J., Smellie, J.L., 1998. Tectonic implications of fore-arc magmatism and generation of high-magnesian andesites: Alexander Island, Antarctica. J. Geol. Soc. 155, 269–280.
Miyashiro, A., 1974. Volcanic rock series in island arcs and active continental margins. Am. J. Sci. 274, 321–355.
Nielsen, S.G., Yogodzinski, G.M., Prytulak, J., Plank, T., Kay, S.M., Kay, R.W., Blusztajn, J., Owens, J.D., Auro, M., Kading, T., 2016. Tracking along-arc sediment inputs to the Aleutian arc using thallium isotopes. Geochim. Cosmochim. Acta 181, 217–237.
O'Neill, H.S.C., 2016. The smoothness and shapes of chondrite-normalized rare Earth element patterns in basalts. J. Petrol. 57, 1463–4508.
Peacock, S.M., 2001. Are the lower planes of double seismic zones caused by serpentine dehydration in subducting oceanic mantle? Geology 29, 299–302.
Penniston-Dorland, S.C., Kohn, M.J., Manning, C.E., 2015. The global range of subduction zone thermal structures from exhumed blueschists and eclogites: rocks are hotter than models. Earth Planet. Sci. Lett. 428, 243–254.
Plank, T., 2005. Constraints from Thorium/Lanthanum on sediment recycling at subduction zones and the evolution of continents. J. Petrol. 46, 921–944.
Plank, T., Cooper, L.B., Manning, C.E., 2009. Emerging geothermometers for estimating slab surface temperatures. Nat. Geosci. 2, 611–615.
Plank, T., Kelley, K.A., Zimmer, M.M., Hauri, E.H., Wallace, P.J., 2013. Why do mafic arc magmas contain ~4 wt% water on average? Earth Planet. Sci. Lett. 364, 168–179.
Poli, S., Schmidt, M.W., 2002. Petrology of subducted slabs. Annu. Rev. Earth Planet. Sci. 30, 207–235.
Portnyagin, M., Hoernle, K., Plechov, P., Mironov, N., Khubunaya, S., 2007. Constraints on mantle melting and composition and nature of slab components in volcanic arcs from volatiles (H_2O, S, Cl, F) and trace elements in melt inclusions from the Kamchatka arc. Earth Planet. Sci. Lett. 255, 53–69.
Ranero, C.R., Morgan, J.P., McIntosh, K., Reichert, C., 2003. Bending-related faulting and mantle serpentinization at the Middle America trench. Nature 425, 367–373.
Rogers, G., Saunders, A.D., Terrell, D.J., Verma, S.P., Marriner, G.F., 1985. Geochemistry of Holocene volcanic rocks associated with ridge subduction in Baja, California, Mexico. Nature 315, 389–392.
Salters, V.J.M., Stracke, A., 2003. Composition of the depleted mantle. Geochem. Geophys. Geosyst. 5. http://dx.doi.org/10.1029/2003GC000597.
Scambelluri, M., Fiebig, J., Malaspina, N., Müntener, O., Pettke, T., 2004. Serpentinite subduction: implications for fluid processes and trace-element recycling. Int. Geol. Rev. 46, 595–613.
Schmidt, M.W., Vielzeuf, D., Auzanneau, E., 2004. Melting and dissolution of subducting crust at high pressures: the key role of white mica. Earth Planet. Sci. Lett. 228, 65–84.
Sims, K.W.W., Maclennan, J., Bilchert-Toft, J., Mervine, E.M., Blusztajn, J., Grönvold, K., 2013. Short length scale mantle heterogeneity beneath Iceland probed by glacial modulation of melting. Earth Planet. Sci. Lett. 379, 146–157.
Sisson, T.W., Grove, T.L., 1993. Experimental investigations of the role of H_2O in calc-alkaline differentiation and subduction zone magmatism. Contrib. Mineral. Petrol. 113, 143–166.
Skora, S., Blundy, J., 2010. High-pressure hydrous phase relations of radiolarian clay and implications for the involvement of subducted sediment in arc magmatism. J. Petrol. 51, 2211–2243.
Spandler, C., Pettke, T., Hermann, J., 2014. Experimental study of trace element release during ultrahigh-pressure serpentinite dehydration. Earth Planet. Sci. Lett. 391, 296–306.
Staudigel, H., 2003. Hydrothermal alteration processes in the oceanic crust. In: Turekian, K.K., Holland, H.D. (Eds.), The Crust. In: Treatise on Geochemistry, vol. 3. Elsevier/Pergamon, Amsterdam/Boston, pp. 511–535.
Stern, C.R., Killian, R., 1996. Role of the subducted slab, mantle wedge and continental crust in the generation of adakites from the Andean Austral Volcanic Zone. Contrib. Mineral. Petrol. 123, 263–281.
Syracuse, E.M., Abers, G.A., 2006. Global compilation of variations in slab depth beneath arc volcanoes and implications. Geochem. Geophys. Geosyst. 7, Q05017. http://dx.doi.org/10.1029/2005GC001045.
Syracuse, E.M., van Keken, P.E., Abers, G.A., 2010. The global range of subduction zone thermal models. Phys. Earth Planet. Inter. 183, 73–90.
Tamura, Y., Gill, J.B., Tollstrup, D., Kawabata, H., Shkuno, H., Chang, Q., Miyazaki, T., Takahashi, N., Hirahara, Y., Kodaira, S., Ishizuka, O., Suzuki, T., Kido, Y., Fiske, R.S., Tatsumi, Y., 2009. Silicic magmas in the Izu–Bonin oceanic arc and implications for crustal evolution. J. Petrol. 50, 685–723.
Tatsumi, Y., Hamilton, D.L., Nesbitt, R.W., 1986. Chemical characteristics of fluid phase released from a subducted lithosphere and origin of arc magmas: evidence from high-pressure experiments and natural rocks. J. Volcanol. Geotherm. Res. 29, 293–309.
Taylor, H.P., Sheppard, S.M.F., 1986. Igneous rocks; I, processes of isotopic fractionation and isotope systematics. Rev. Mineral. Geochem. 16, 227–271.
Tenthorey, E., Hermann, J., 2004. Composition of fluids during serpentinite breakdown in subduction zones: evidence for limited boron mobility. Geology 32, 865–868.
Tollan, P.M.E., Bindeman, I., Blundy, J., 2012. Cumulate xenoliths from St. Vincent, Lesser Antilles Island Arc: a window into upper crustal differentiation of mantle-derived basalts. Contrib. Mineral. Petrol. 163, 189–208.
Turner, S., Hawkesworth, C., van Calsteren, P., Heath, E., Macdonald, R., Black, S., 1996. U-series isotopes and destructive plate margin magma genesis in the Lesser Antilles. Earth Planet. Sci. Lett. 142, 191–207.
Ulmer, P., Trommsdorff, V., 1995. Serpentine stability to mantle depths and subduction-related magmatism. Science 268, 858–861.
van Keken, P.E., Hacker, B.R., Syracuse, E.M., Abers, G.A., 2011. Subduction factory: 4. Depth-dependent flux of H_2O from subducting slabs worldwide. J. Geophys. Res., Solid Earth 116.
Walowski, K.J., Wallace, P.J., Hauri, E.H., Wada, I., Clynne, M.A., 2015. Slab melting beneath the Cascade Arc driven by dehydration of altered oceanic peridotite. Nat. Geosci. 8, 404–408.
Wanless, V.D., Perfit, M.R., Ridley, W.I., Klein, E., 2010. Dacite petrogenesis on mid-ocean ridges: evidence for oceanic crustal melting and assimilation. J. Petrol. 51, 2377–2410.
Yamaoka, K., Fukao, Y., Kumazawa, M., 1986. Spherical shell tectonics: effects of sphericity and inextensibility on the geometry of the descending lithosphere. Rev. Geophys. 24, 27–53.
Yogodzinski, G.M., Kelemen, P.B., 1998. Slab melting in the Aleutians: implications of an ion probe study of clinopyroxene in primitive adakite and basalt. Earth Planet. Sci. Lett. 158, 53–65.
Yogodzinski, G.M., Volynets, O.N., Koloskov, A.V., Seliverstov, N.I., Matvenkov, V.V., 1994. Magnesian andesites and the subduction component in a strongly calc-alkaline series at Piip Volcano, far western Aleutians. J. Petrol. 35, 163–204.
Yogodzinski, G.M., Kay, R.W., Volynets, O.N., Koloskov, A.V., Kay, S.M., 1995. Magnesian andesite in the western Aleutian Komandorsky region: implications for slab melting and processes in the mantle wedge. Geol. Soc. Am. Bull. 107, 505–519.
Yogodzinski, G.M., Lees, J.M., Churikova, T.G., Dorendorf, F., Wörner, G., Volynets, O.N., 2001. Geochemical evidence for the melting of subducting oceanic lithosphere at plate edges. Nature 409, 500–504.
Yogodzinski, G.M., Brown, S.T., Kelemen, P.B., Vervoort, J.D., Portnyagin, M., Sims, K.W.W., Hoernle, K., Jicha, B., Werner, R., 2015. The role of subducted basalt in the source of island arc magmas: evidence from seafloor lavas of the western Aleutians. J. Petrol. 56, 441–492.